Water and Wastewater, Vol. , No. , pp:

Ultrasound-Enhanced Alkaline Modification of Wheat Straw for Efficient Removal of Industrial Ionic Dyes

Ramin Alizadeh[1], Elham Jalilnejad[2*], Reza Rafiee[3]

1. MSc. Student, Faculty of Chemical Engineering, Urmia University of Technology, Urmia 17165-57166, Iran
2. Assoc. Prof., Faculty of Chemical Engineering, Urmia University of Technology, Urmia 17165-57166, Iran (Corresponding Author) e.jalilnejad@uut.ac.ir
3. Assist. Prof., Faculty of Chemical Engineering, Urmia University of Technology, Urmia 17165-57166, Iran

https://doi.org/10.22093/wwj.2025.554485.3521 **Original Paper**

Abstract

This study aims to support eco-friendly wastewater treatment by converting lignocellulosic waste into valuable biosorbents, thereby contributing to sustainable waste management technologies. Wheat straw and its ash were examined as low-cost adsorbents for the removal of industrial ionic dyes, including cationic methylene blue and anionic methyl orange. To enhance adsorption performance, several surface modification approaches, including alkaline, acidic, and ultrasound-assisted treatments, were evaluated. The structural and surface characteristics of the modified materials were analyzed using Brunauer–Emmett–Teller and Fourier transform infrared spectroscopy techniques. Among all prepared adsorbents, the sodium hydroxide–ultrasound-modified ash (WSA-U-NaOH) exhibited the highest adsorption efficiency under initial testing conditions (25 mg/L dye), achieving capacities of 12.38 mg/g for MB and 4.47 mg/g for MO, evidencing a synergistic enhancement attributable to the combined effects of alkaline activation and ultrasonic cavitation. Optimization using the Taguchi model revealed that the maximum adsorption capacity for MB (53.29 mg/g) occurred at pH=12 with 0.05 g of adsorbent and an initial MB concentration of 75 mg/L after 45 minutes. For MO, optimal conditions (pH=2, 0.05 g adsorbent, and 75 mg/L MO) produced a capacity of 22.36 mg/g after 60 minutes. The adsorbent exhibited a markedly higher affinity toward the cationic dye, consistent with electrostatic interactions governed by surface charge characteristics. Kinetic analyses showed that adsorption followed the pseudo-second-order model, suggesting chemisorption as the dominant rate-controlling step. Equilibrium data were best fitted by the Freundlich isotherm, indicating heterogeneous multilayer adsorption. Thermodynamic parameters confirmed that the biosorption of both dyes was spontaneous and endothermic.

Keywords:
Lignocellulosic Waste, Wheat Straw, Adsorption, Industrial Dye, Surface Modification, Ultrasound.

Received: Dec. 3, 2024
Revised: Jan. 12, 2025
Accepted: Feb. 15, 2025

To cite this article:
Alizadeh, R., Jalilnejad, E., Rafiee, R., 2025. Ultrasound-enhanced alkaline modification of wheat straw for efficient removal of industrial ionic dyes. *Water and Wastewater*, (In press). https://doi.org/10.22093/wwj.2025.554485.3521.

Use your device to scan and read the article online

1. Introduction

In recent years, environmental pollution caused by a high concentration of various pollutants, such as dyes, heavy metals, toxic ions, mineral anions, micropollutants, and organic compounds like phenols, pesticides, and detergents, has emerged as a significant global concern. The release of these toxic pollutants into natural waters has severely disrupted ecological balance, causing harmful effects on plant and animal life (Alizadeh et al., 2019; Jalilnejad et al., 2024).

Among the sources of pollution, dyes used in industries such as textiles, paper, printing, dyeing, plastics, and leather are particularly prevalent and require advanced remediation methods to avoid environmental pollution. The wastewater from these industries often contains large amounts of colored waste materials. Synthetic dyes, in particular, pose a serious environmental threat and are considered hazardous to human health. Additionally, the presence of pigments in water systems reduces oxygen levels and light penetration, adversely impacting photosynthesis in plants and aquatic organisms (Alizadeh et al., 2026; Forouzandeh-Malati et al., 2022; Hemmatzadeh et al., 2024; Jalilnejad et al., 2025; Ma et al., 2025).

To remove dyes from wastewater, various separation methods have been employed, including electrochemical processes, ion exchange resins, filtration, sedimentation, coagulation, photocatalytic degadation (specially visible-light-driven systems), and membrane-based techniques like reverse osmosis and nanofiltration. However, many of these methods have significant limitations, such as incomplete pollutant removal, high equipment costs, energy consumption, and the generation of hazardous by-products (Aghaeinejad Meybodi et al., 2024; Dawi and Padervand, 2025; Heidarpour et al., 2020; Hokkanen et al., 2016; Padervand et al., 2021; Ramrakhiani et al., 2016; Yaghoobi Rahni and Younesi, 2025).

Among the purification methods available, adsorption has been highly successful in removing dyes, heavy metals, and other contaminants. However, conventional adsorbents like activated carbon, clay, silica gel, coal, chitosan, and bentonite often involve high costs and may be inefficient in removing pollutants at low concentrations. In some cases, they also result in sludge production. As a result, considerable research has been devoted to identifying more efficient and cost-effective adsorbents. Recently, lignocellulosic materials derived from wood and agricultural waste have gained attention for their ability to adsorb both organic and inorganic pollutants. These materials offer comparable performance to other natural adsorbents and provide the added advantage of transforming waste products into valuable resources (Alizadeh et al., 2024; De Quadros Melo et al., 2016).

Although unmodified cellulose has limited adsorption capacity and variable physical stability, it is renewable, biodegradable, affordable, and contains numerous active hydroxyl groups. However, to improve the adsorption efficiency of lignocellulosic biomass, it is necessary to modify the material using various methods. These modification techniques can be classified into four categories: physical, chemical, physicochemical, and biological (Alizadeh et al., 2022; Ramrakhiani et al., 2016).

The choice of modification method depends on the specific application of the lignocellulosic material in different fields. For example, biobased-hydrogels are studied in various works for their excellent adsorption capacity, attributed to their swelling ability and porous structure, which allow solutes to diffuse rapidly into their matrices. This makes them an effective and eco-friendly option for dye removal, generating significant research interest in their use as cost-effective adsorbents (Yang et al., 2022).

In the study by Zhang et al., an innovative and effective upcycling strategy was investigated in which low-quality cotton fibers were transformed into high-value hydrogel biosorbents while maintaining excellent dye adsorption performance (Zhang et al., 2024).

In the research carried out by Jawad et al., coconut shell underwent chemical treatment with sulfuric acid (H_2SO_4) to create acid-functionalized biosorbent, which was effectively utilized for removing methylene blue[1] dye from water (Jawad et al., 2020).

Akar et al. explored the biosorption capabilities of sugar-beet pulp, which were enhanced through modification with quaternary ammonium-salt to assess its potential in wastewater decolorization (Akar et al., 2015). The surfactant-modified biosorbent exhibited strong performance in removing Acid Red 1. Silva et al. chemically altered cellulose using phthalic anhydride and diethylenetriamine for dye sorption, achieving adsorption capacities of 65.45 mg/g for methyl orange[2] and 56.69 mg/g for eosin (Silva et al., 2018). Wu et al. employed microwave-assisted alkalization and acid oxidation pretreatments to develop novel wheat straw adsorbents for efficient removal of Cd (II) from simulated waterlogged paddy soil (Wu et al., 2019). Their findings indicated that wheat straw pretreated with microwave-assisted soaking in NaOH and ethanol solution demonstrated the highest Cd (II) removal efficiency of 96.4% under specific conditions. Overall, modifying cellulose is crucial for improving its structural stability and adsorption effectiveness towards pollutants.

Growing concerns over dye-contaminated wastewater have intensified the search for low-cost, sustainable, and high-performance biosorbents. In this study, wheat straw, a readily available lignocellulosic agricultural waste, and its ash were employed as precursor materials for the adsorption of cationic MB and anionic MO dyes. The work specifically evaluates the effectiveness of alkaline, acidic, and ultrasound-assisted modification techniques in enhancing the structural and surface properties of the biosorbent. Using

[1] Methylene Blue (MB)

[2] Methyl Orange (MO)

a systematic experimental design approach, the study identifies the optimal operating conditions (pH, initial dye concentration, and adsorbent dosage) that maximize dye removal efficiency and adsorption capacity. Comprehensive characterization through Fourier Transform Infrared Spectroscopy[1] and Brunauer–Emmett–Teller[2] analyses elucidates the chemical and textural changes induced by each modification method. Kinetic, isotherm, and thermodynamic models were further applied to clarify the adsorption mechanism, rate-controlling steps, and energetic nature of the process. Overall, the study demonstrates an effective valorization pathway for wheat straw waste while providing an environmentally friendly and economically viable solution for wastewater dye removal.

2. Materials and methods

2.1. Adsorbent preparation

Wheat straw was collected from a local farm in Urmia, Iran. It was washed three times with distilled water to eliminate dust and surface contaminants. The washed straw was then dried in an oven at 60 °C for 24 hours. The dried straw was ground into powder using a mechanical grinder, reducing the particle size to a few millimeters. Straw ash was produced by burning pre-washed straw in an open environment. The ash was washed and dried following the same procedure as the straw.

2.2. Alkali treatment

Wheat straw and ash were treated with NaOH and KOH. For this purpose, 100 ml of NaOH (0.5 M) and 100 ml of KOH (0.1 M) were each added to 5 grams of wheat straw in separate Erlenmeyer flasks (200 ml). The modification process was performed for 2 hours at room temperature, with stirring at 300 rpm. The same procedure was followed for straw ash. After modification, the samples were separated from the solution by filtration and washed with distilled water until they reached a neutral pH, then dried in an oven at 60 °C for 24 hours.

2.3. Acid treatment

The acid treatment of wheat straw and ash was done using H_2SO_4, HCl, H_3PO_4, and $C_6H_8O_7$. For each acid, 100 ml of H_2SO_4 (1 M), HCl (0.1 M), H_3PO_4 (35% wt) and $C_6H_8O_7$ (0.6 M) were added to 5 gr of straw in separate 200 ml Erlenmeyer flasks. The modification process was carried out for 2 hours with stirring at 300 rpm, except for H_3PO_4, which required 24 hours at ambient temperature. Straw ash was also modified using the same procedure. After treatment, the samples were filtered, washed with distilled water until neutral pH, and dried at 60 °C for 24 hours.

2.4. Ultrasound-based modification

Ultrasonic modification was applied after identifying the most effective adsorbents from the alkali and acid treatments. The unmodified straw and ash served as control samples. 5 gr of the optimal adsorbent was mixed with 500 ml of distilled water in an 800 ml beaker and stirred for 10 minutes. The solution was placed in an ice bath to prevent heating during ultrasound treatment (480 W power, 24 kHz frequency, and 60% fluctuation) for 1 hour. After treatment, the samples were separated from the solution and dried at 60 °C for 24 hours.

2.5. Determining the point of zero charge (pH_{pzc}) of the adsorbent

The surface charge of the optimum adsorbent was determined using the salt titration method. A 0.01 M NaCl solution was prepared, and its pH was adjusted to a range of 2 to 12 by adding KOH or HCl. 50 ml of NaCl solution at various pH levels were added to 100 ml beakers containing 0.1 g of adsorbent. The solutions were left for 24 hours, after which the final pH was measured with a pH-meter.

2.6. Adsorption experiments

2.6.1. Preparation of adsorption solutions

Dye solutions for the adsorption tests were prepared by diluting stock solutions of MB and MO (500 mg/L concentration). The pH was adjusted using KOH and 0.1 M HCl. The maximum wavelength (λ_{max}) of MB and MO was determined with a spectrophotometer, measuring at 671 and 472 nm, respectively.

2.6.2. Batch adsorption of MB and MO

To assess the effectiveness of raw wheat straw, ash, and modified adsorbents, the adsorption process was conducted for both dyes. The experimental conditions were: adsorbent dose of 0.1 g, initial dye concentration of 25 ppm, solution volume of 50 ml, stirring speed of 300 rpm, pH of 7, and room temperature. Samples were taken every 15 min for both wheat straw and ash every 15 minutes until equilibrium was reached. Optimal adsorbents were determined based on dye removal. Ultrasound modification was then applied to Unmodified wheat straw (WS-Unmodified), Unmodified ash (WSA-Unmodified), NaOH-modified wheat straw (WS-U-NaOH), NaOH-modified ash (WSA-U-NaOH), H_3PO_4-modified wheat straw (WS-U-H_3PO_4), and H_3PO_4-modified ash (WSA-U-H_3PO_4) under the same experimental conditions.The adsorption capacity at time t (q_t) (Eq. 1) and removal percentage (Re%) (Eq. 2) were calculated using the following equations

[1] Fourier Transform Infrared Spectroscopy (FTIR)
[2] Brunauer–Emmett–Teller (BET)

$$q_t = \frac{(C_0 - C_t)V}{M} \quad (1)$$

$$Re\% = \frac{(C_0 - C_t)}{C_0} \times 100\% \quad (2)$$

Where

C_0 (mg/L) is the initial dye concentration, C_t (mg/L) is the dye concentration at time t, V (L) is the solution volume, and M (g) is the mass of the adsorbent (Guo et al., 2019). Two replicates were conducted in the experiments and the mean value is used to characterize the adsorption process.

2.7. Design of experiments via Taguchi method

The Taguchi method, a simple yet powerful tool for optimizing processes and reducing experimental runs, was employed to investigate factors affecting adsorption (Abdolkarimi Mahabadi and Bayat, 2024; Deniz, 2013). The independent parameters (pH, adsorbent dose, and initial dye concentration) were examined at different levels (Table 1-a). For MB and MO removal, 9 tests were designed (Table 1-b), involving 50 ml of dye solutions with concentrations of 25, 50 and 75 mg at pH levels of 2, 7 and 12, and adsorbent dosages of 0.05, 0.1 and 0.15 gr. The tests were conducted at room temperature, stirring at 300 rpm for the optimal contact times (45 minutes for MB and 60 minutes for MO).

2.8. Adsorption kinetics

Kinetic models were used to analyze adsorption dynamics and the factors influencing the adsorption rate. Models such as pseudo-first-order, pseudo-second-order, and intraparticle diffusion (Table 2) were applied to adsorption systems via Microsoft Excel (Idan et al., 2018; Kecili and Hussain, 2018; Tejada-Tovar et al., 2021). The best-fitting model was determined by comparing correlation coefficients (R^2) and sum of squared errors[1]. The larger the R^2 and the smaller the SSE, the better the model fits the data. The SSE is calculated by

$$SEE = \sqrt{\sum \frac{[(exp.Data - cal.Data)/exp.Data]^2}{n}} \quad (3)$$

Where

n is the number of the experiments. Using the optimal conditions from the Taguchi design, different kinetic models were tested for MB and MO over 45 and 60 minutes, with 5-minute intervals.

2.9. Adsorption isotherms

Adsorption isotherms describe the relationship between the adsorbate concentration and the adsorbent's capacity. Common isotherm models, such as Langmuir, Freundlich, and Temkin (Table 3), were used to analyze the equilibrium adsorption of MB and MO based on the optimal conditions identified by the Taguchi design method (Han et al., 2010). The linear forms of the three utilized models are given by the equations presented in Table 3 (Gouamid et al., 2013; Hong et al., 2009; Jain and Gogate, 2017; Salman et al., 2015). Model fitting for isotherms was performed in Microsoft Excel Solver by reducing the SSE to its minimum.

2.10. Adsorption thermodynamics

Thermodynamic studies assess whether adsorption processes are spontaneous. Gibbs free energy change (ΔG°), enthalpy (ΔH°), and entropy (ΔS°) were calculated using the following equations (Eqs. 4-6)

$$\Delta G° = -RT \ln(K_d) \quad (4)$$

$$\Delta G° = \Delta H° - T\Delta S° \quad (5)$$

$$\ln(K_d) = \frac{\Delta S°}{R} - \frac{\Delta H°}{RT} \quad (6)$$

Where

R is the universal gas constant (8.314 KJ/mol K), and T is the temperature (K). The enthalpy and entropy changes were determined from the slope and intercept of the linear plot of lnK° versus 1/T (Gouamid et al., 2013; Hong et al., 2009). Dye adsorption was examined at 25, 35, and 45 °C using 50 ppm adsorbate in 100 ml volumetric flasks, stirred at 300 rpm.

3. Results and discussion

3.1. FTIR analysis

The FTIR spectra of wheat straw and ash samples presented in Fig. 1 have been used to compare the functional groups of the adsorbents and the effects of acid and base modifications on them. The absorption peaks in the range of 3403-3444 cm^{-1} correspond to the stretching vibrations of the OH groups, and the reduction in intensity observed in the samples modified with NaOH is likely due to dehydration and further removal of OH groups in lignin and hemicellulose. The peaks observed in the range of 2928-2913 cm^{-1} are attributed to the C-H stretching vibrations of the aliphatic chain structure of lignin, which shows a weak intensity and is almost eliminated in the ash samples due to lignin removal. The peak at 1734 cm^{-1} corresponds to the ester groups of wheat straw, which were removed after modification, and this peak was also not observed in the ash samples. The peaks appearing in the range of 1633-1629 cm^{-1} are related to the C=O groups of carboxylic acids or their esters. As observed, the intensity of this peak decreased after the modification of straw and ash with NaOH, which may be due to the degradation of cell wall compounds, including proteins and some organic

[1] Sum of Squared Errors (SSE)

Table 1. a) Factors and their level conducted in the experiment, b) Experimenal design matrix and expected response

a)

Independent variables	Code	Level 1	Level 2	Level 3
pH	A	2	7	12
Adsorbent dosage (g)	B	0.05	0.1	0.15
Dye initial concentration (mg/L)	C	25	50	75

b)

Run No.	Adsorption process variables			Adsorption efficiency			
				MB		MO	
	A	B	C	Removal (%)	Ads. capacity (mg/g)	Removal (%)	Ads. capacity (mg/g)
1	2	0.05	25	69.10	17.28	35.09	7.78
2	2	0.1	50	71.11	17.77	50.10	12.52
3	2	0.15	75	80.07	20.01	63.81	15.95
4	7	0.05	50	62.06	31.03	28.44	14.72
5	7	0.1	75	69.25	25.96	31.33	11.75
6	7	0.15	25	98.65	8.22	46.61	3.88
7	12	0.05	75	71.05	53.29	16.27	12.21
8	12	0.1	25	97.80	12.22	27.04	3.38
9	12	0.15	50	98.58	16.43	23.30	3.88

Table 2. Kinetic parameters related to dye adsorption

Kinetic model	Parameter	MB	MO
Pseudo-first-order	k_1 (1/min)	0.115	0.06
$\ln(q_e-q_t)=\ln q_e-k_1 t$	q_e (mg/g)	24.48	15.61
	R^2	0.97	0.93
Pseudo-second-order	k_2 (g/(mg.min))	0.011	0.002
$\frac{t}{q_t}=\frac{1}{k_2 q_e^2}+\frac{1}{q_e}t$	q_e (mg/g)	55.55	21.69
	R^2	0.99	0.96
Intra-particle diffusion	k_{id} (mg/(g.min$^{1/2}$))	4.35	2.26
$q_t = k_{id}(t)^{1/2} + C$	C (mg/g)	30.72	0.91
	R^2	0.95	0.95

components. However, the intensity of this peak in the modification with H_3PO_4 indicates less degradation of glycosidic bonds and hydroxyl groups of hemicellulose. The absorption peaks in the range of 1094-1041 cm^{-1} are related to the C-O-C stretching vibrations, and the increase in intensity in the samples modified with H_3PO_4 is associated with the P=O group in phosphate, the O-C bond in P-O-C, or the P=OOH bond (Silva et al., 2018; Wu et al., 2019). The peak observed at 903 cm^{-1} corresponds to the phosphorus-oxygen groups, and the broad peak in the range of 720-593 cm^{-1} is due to the oxygen group of H_3PO_4.

3.2. BET analysis

The specific surface area of an adsorbent plays a crucial role in determining its adsorption capacity. Table 4 provides information on the specific surface area and pore volume of adsorbents that have been modified with NaOH and H_3PO_4, as well as wheat straw and ash in their unmodified state. Based on the data obtained, both

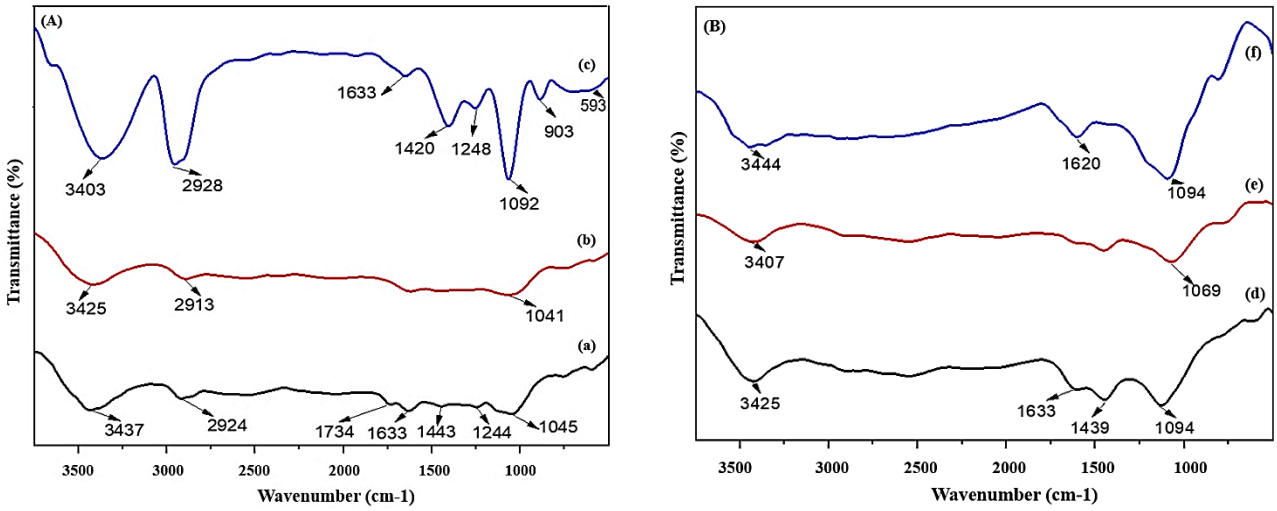

Fig. 1. FTIR spectra of (A) wheat straw: a-unmodified, b- NaOH modified, c- H_3PO_4 modified and (B) wheat straw ash: d- unmodified, e- NaOH modified, f- H_3PO_4 modified

Table 3. Isotherm parameters related to MB adsorption at different initial dye concentrations

Isotherm model	Parameter	MB	MO
Langmuir isotherm	q_m (mg/g)	57.14	15.13
$\frac{1}{q_e}=\frac{1}{q_m}+\frac{1}{q_m K_L}\frac{1}{C_e}$	K_L (L/mg)	0.24	0.39
	R^2	0.95	0.92
Freundlich isotherm	K_f (mg/g)	13.32	6.92
$\log q_e = \log K_F + (\frac{1}{n})\log C_e$	1/n	0.46	0.23
	R^2	0.99	0.98
Temkin isotherm	k_T (L/g)	1.43	6.27
$q_e = \beta \ln K_T + \beta \ln C_e$	β (J/mol)	15.48	2.68
	R^2	0.92	0.94

q_m: The maximum adsorption capacity, q_e (mg/g): The equilibrium adsorption capacity
C_e (mg/L): The equilibrium concentration, K_L: The Langmuir constant, C_0 (mg/L): The initial dye concentration
K_F and n: The Freundlich constants, K_T (L/g): The Temkin constant, β (J/mol) Is the adsorption energy

Table 4. BET analysis results of unmodified and modified WS and its ash

	Specific area (m^2/g)	Pore volume (cm^3/g)
NaOH-WS	3.266	0.0043
H_3PO_4-WS	1.750	0.0028
Unmodified-WS	0.588	0.0020
NaOH-WSA	36.153	0.0988
H_3PO_4-WSA	9.751	0.0324
Unmodified-WSA	9.426	0.0266

alkaline and acidic modifications resulted in an increase in the specific surface area and pore volume of wheat straw and its ash compared to unmodified samples. The most effective modification was observed with NaOH, which increased the specific surface area of straw from 0.5884 m^2/g to 3.2662 m^2/g and ash from 9.426 m^2/g to 36.153 m^2/g. This increase in specific surface area led to enhanced adsorption capacity of the modified adsorbents.

3.3. Impact of different modifications on dye removal efficiency in various samples

3.3.1. The effect of alkaline and acidic modification on wheat straw

Fig. 2 illustrates the impact of alkaline and acidic treatments on wheat straw for dye removal over varying contact times. The experiments were conducted under consistent conditions of a dye concentration of 25 mg/L, an adsorbent amount of 0.1 g, pH=7, and ambient temperature. In Fig. 2-a, it is evident that the NaOH-modified adsorbent (WS-NaOH) exhibited the highest efficiency in removing MB, achieving a removal efficiency of 96. 4%. In comparison, the H_3PO_4-modified (WS-H_3PO_4) sample showed lower removal efficiency, along with the H_2SO_4, HCl, and $C_6H_8O_7$-modified samples, which can be attributed to their reduced pore volume and specific surface area. The lower removal percentage of the acid-modified adsorbents may be due to the cationic nature of the MB dye, leading to repulsion between the dye molecules and the adsorbent surface. Through FTIR and BET analysis, it was determined that NaOH modification played a more effective role in removal by enhancing lignin and hemicellulose removal, disrupting cell wall components, and increasing specific surface area and pore volume.

In Fig. 2-b, the impact of alkaline and acidic modification on the efficacy of wheat straw in removing MO is presented. The findings demonstrate that both alkaline and acidic modifications enhance the adsorption efficiency of wheat straw. The NaOH-modified adsorbent achieved the highest removal percentage at 25.6%, followed by the H_3PO_4-modified adsorbent at 18.66%, compared to 3.9% for the unmodified adsorbent. The increased removal of MO can be attributed to the higher porosity and specific surface area of the NaOH-modified adsorbent (WS-NaOH) compared to other straw samples. Additionally, the adsorption by the H_3PO_4-modified adsorbent was notable due to the introduction of new functional groups on the wheat straw's surface. Similar results, indicating enhanced efficiency in removing the anionic dye of acid-violet 17 with lignocellulosic adsorbent modified with NaOH compared to H_2SO_4-modified adsorbent, were also reported by Jain and Gogate (Jain and Gogate, 2017).

3.3.2. The effect of alkaline and acidic modification on wheat straw ash

Fig. 3 depicts the impact of alkaline and acidic modifications on wheat straw ash for dye removal. The results indicate that modification with NaOH, KOH and H_3PO_4 positively influenced the MB adsorption process (Fig. 3-a), enhancing removal efficiency and adsorption capacity. Conversely, other acid-modified adsorbents led to decreased dye adsorption due to repulsion between the pollutant and adsorbent surface, as well as shorter modification times compared to H_3PO_4. This trend differed in MO adsorption, where all modified adsorbents increased the percentage of MO removal compared to unmodified ash (Fig. 3-b). The use of straw ash improved adsorption rate and early equilibrium due to enhanced accessibility of dye molecules to adsorption sites. In particular, NaOH-modified adsorbent (WSA-NaOH) exhibited the highest percentage of dye removal for MB (97.1%) and MO (31.6%), attributed to its porosity and high specific surface area (36.153 m^2/g) compared to unmodified (9.426 m^2/g) and phosphoric acid-modified (9.751 m^2/g) samples. Based on the data collected regarding dye removal, it was found that the most effective methods for modifying wheat straw and ash involved the use of NaOH as alkaline modification. This modification significantly enhanced the removal of MB and MO as cationic and anionic dyes, respectively (Song et al., 2023). Additionally, ultrasound treatment was applied in the next step to further improve the efficiency and adsorption capacity.

3.3.3. The effect of ultrasound modification on wheat straw and its ash

Ultrasound modification alters the morphology and structure of the adsorbent, leading to increased exfoliation, surface cleaning, and enhanced porosity and permeability. The impact of ultrasound modification on the efficiency of both unmodified straw and ash adsorbents, as well as optimally modified adsorbents, was assessed. Fig. 4 illustrates the adsorption process of dyes at a concentration of 25 mg/L, with an adsorbent amount of 0.1 g, pH=7, and at ambient temperature. Based on the data presented in Figs. 4-a and 4-b, the highest adsorption capacity for MB was achieved by ash when subjected to combined modification with NaOH and ultrasound (WSA-U-NaOH), reaching a value of 12.38 mg/g. These results indicated that the combined modification of ash was more effective in MB removal compared to wheat straw modified with ultrasound (WS-U). The adsorption capacities of the other samples followed the order:

WSA-U-NaOH > WS-U-NaOH > WSA-U > WS-U-H_3PO_4 > WSA-U-H_3PO_4

Furthermore, as shown in Figs. 4-c and 4-d, the efficiency of the ash modified with sodium hydroxide

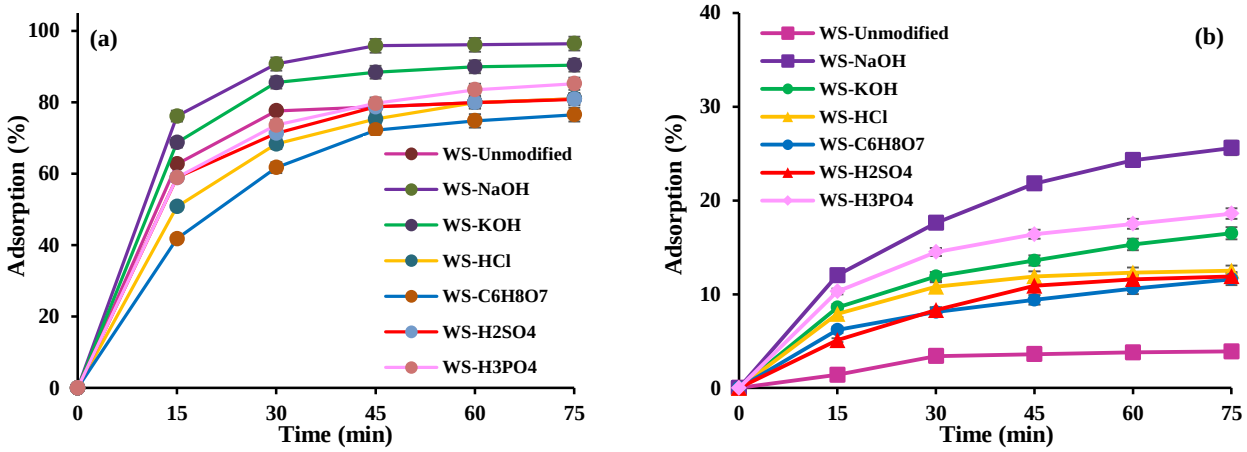

Fig. 2. Effect of acidic and alkaline modification of wheat straw on adsorption of (a) MB and (b) MO dyes (adsorbent dosage=0.1 g/L, initial dye concentration=25 mg/L, pH=7, stirring speed=300 rpm)

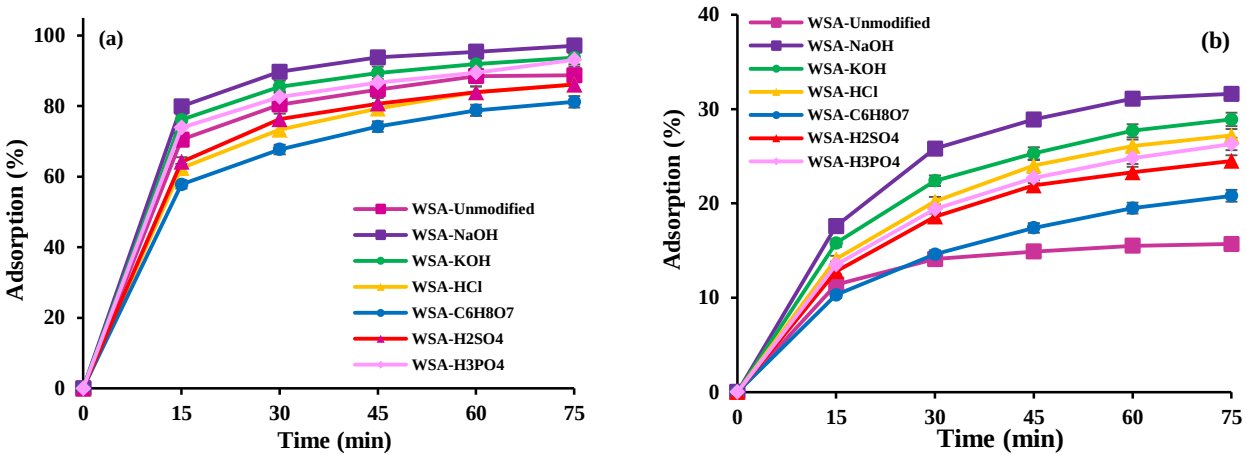

Fig. 3. Effect of acidic and alkaline modification of wheat straw ash on adsorption of (a) MB and (b) MO dyes (adsorbent dosage=0.1 g/L, initial dye concentration=25 mg/L, pH=7, stirring speed=300 rpm)

and ultrasound (WSA-U-NaOH) in removing MO surpassed that of the other samples (q_t=4.47 mg/g). Ultrasound modification not only increased the adsorption capacity of the samples but also enhanced adsorption speed and facilitated early equilibrium (Hu et al., 2024).

Ultrasound enhanced the efficiency of alkali modification through the acoustic cavitation mechanism, where the collapse of microbubbles produces microjets and shock waves that disrupt the lignocellulosic matrix. These intense mechanical forces open clogged pores, remove surface debris, and facilitate deeper penetration of NaOH, leading to greater delignification and exposure of active functional groups. As a result, a clear synergistic improvement in porosity, surface area, and adsorption capacity was observed for the ultrasound–alkali modified adsorbent (Akar et al., 2015; Hokkanen et al., 2016; Hu et al., 2024).

Through the evaluation of various modification methods for dye removal, it was concluded that WSA-U-NaOH exhibited superior adsorption capacity compared to the other adsorbents studied. Subsequently, additional parameters influencing the adsorption process were examined on this specific adsorbent for the adsorption of MB and MO.

3.4. Adsorption experiments

3.4.1. Point of zero charge (pH_{pzc})

The zero point of charge is an important factor that determines the linear sensitivity range of pH as well as the type of active surface sites of the adsorbent and its surface capacity. According to Fig. 5, for the ash modified with sodium hydroxide and ultrasound, a pH_{pzc} of 7.5 was obtained. At pH>pH_{pzc}, the adsorbent surface carries a negative charge, and at pH<pH_{pzc}, it becomes positively charged.

3.4.2. Effect of contact time

Fig. 6 depicts the impact of adsorbent contact time on the removal of MB and MO dyes using an adsorbent

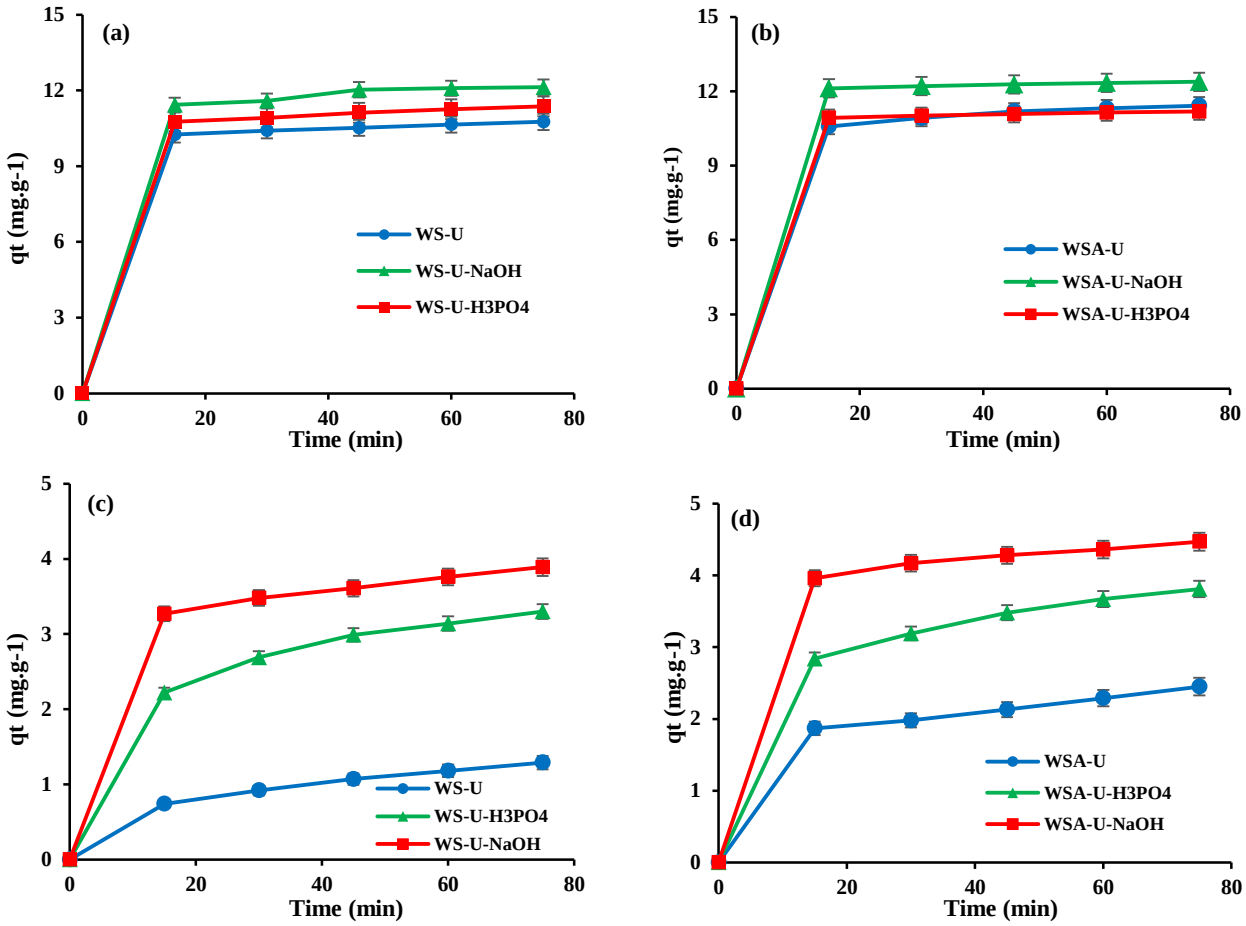

Fig. 4. Effect of ultrasound treatment on adsorption of (a,b) MB, (c,d) MO dyes (adsorbent dosage=0.1 g/L, initial dye concentration=25 mg/L, pH=7, stirring speed=300 rpm)

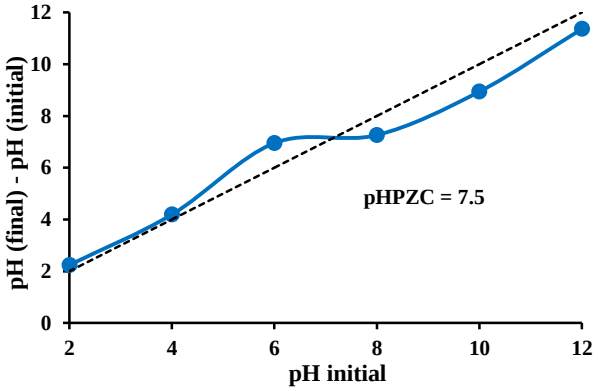

Fig. 5. Impact of pH on surface charge density (pH_{pzc}) of WSA-U-NaOH

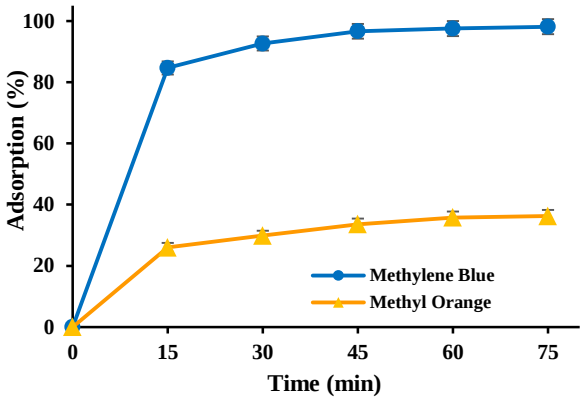

Fig. 6. Effect of contact time on adsorption of MB and MO by WSA-U-NaOH adsorbent (adsorbent dosage=0.1 g/L, initial dye concentration=25 mg/L, pH=7, stirring speed=300 rpm)

amount of 0.1 g, a dye concentration of 25 mg/L, pH=7, a volume of 50 ml, and ambient temperature. The adsorption rate of the adsorbent was notably rapid within the initial 30 minutes for both dyes, followed by a slower rate between 30 to 60 minutes until saturation was achieved. The optimal contact time for MB was determined to be 45 min, while for MO, it was 60 min. As time progressed and the adsorbent surface sites became saturated, the removal process reached a constant value.

3.4.3. Experimental design results

The effect of different parameters, including pH, adsorbent dosage, and pollutant concentration, on dye removal was investigated using the Taguchi experimental design method. The test conditions and removal results of each sample, based on removal percentage and adsorption capacity, are presented in Table 1-b. The Qualitek-4 software was utilized to analyze the results and determine the optimal conditions for dye removal.

3.4.3.1. Optimal conditions for MB adsorption

The results of the analysis of variance[1] for MB adsorption, focusing on removal efficiency and adsorption capacity, are detailed in Table 5. The data indicates that the dye concentration exerts a more significant influence on the adsorption process compared to the pH of the solution and the adsorbent dosage used regarding the adsorption capacity as response.

Fig. 7 illustrates the impact of these parameters at different levels. In Fig. 7-a, the adsorption rate of MB dye on the adsorbent surface is influenced by the pH of the solution, likely attributed to the cationic nature of MB^+ in aqueous solutions. The graph demonstrates that the adsorption capacity is minimum at pH=2 and peaks at pH=12. This behavior is a result of an abundance of H^+ ions in an acidic environment leading to repulsion and reduced adsorption, while the presence of OH^- ions in an alkaline environment enhances dye adsorption. Fig. 7-b shows a decrease in adsorption capacity with an increase in adsorbent dosage at constant concentration and volume, possibly due to the saturation of adsorption sites caused by particle overlap effects, including particle aggregation on the adsorbent surface. In Fig. 7-c, the most significant impact on adsorption capacity was observed when the pollutant concentration was increased. The findings indicated that as the initial concentration of the MB solution increased, the removal efficiency decreased while the equilibrium adsorption capacity increased. This suggests that as the concentration rises, the driving force for mass transfer also increases, leading to greater dye adsorption. The optimization analysis was conducted with respect to both adsorption capacity and removal efficiency and the target criterion was set as maximum values for the two responses.

The optimum adsorption conditions obtained were presented in Table 6. At optimal conditions, the MB removal efficiency was found to be 114.7%. The predicted value by the software (114.7%) can be interpreted as the maximum possible adsorption of MB ions from the aqueous solution. However the experimental values obtained at optimum conditions for MB and MO removals were 98.85% and 67.92% respectively, showing good agreement between the experimental values and those predicted from the models.

3.4.3.2. Optimal conditions for MO adsorption

The ANOVA results in Table 5 indicate that pH has the most significant impact on the adsorption process, regarding removal efficiency as response. The adsorbent dosage and dye concentration of the solution also contributed to the process, with effects of 26.59% and 14.45%, respectively. Fig. 7-d shows that higher adsorption of MO occurred at acidic pH, possibly attributed to electrostatic attraction forces between dye anions and positive ions. This sensitivity is influenced by the ionization degree of functional groups in the adsorption sites and substances present in the solution. In Fig. 7-e, increasing the adsorbent dosage to 0.1 g led to a slight increase in adsorption capacity due to the availability of more adsorption sites. However, at a dosage of 0.15 g, the adsorption capacity did not increase, likely due to the saturation of adsorption sites. Examination of the concentration of MO adsorption in Fig. 7-f revealed a similar effect to the MB adsorption process.

Using the Taguchi model, the optimal adsorption conditions for MO removal were identified as shown in Table 6. At optimal conditions, the MO removal efficiency was found to be 71.94%.The recounted adsorption percentage removal and optimum adsorption capacity at optimum conditions based on experimental values for removing MO were 67.92% and 22.36 mg/g, respectively, which showed good agreement between predicted and experimental data. Through the ANOVA data and parameter investigation in this study, it was concluded that the efficiency of the optimal adsorbent in removing the cationic dye MB surpassed that of the anionic dye MO, promoting the industrial application of modified wheat straw at achieved optimal conditions. The adopted approach was very effective and the results obtained indicated that the Taguchi method provided high percentage of MB removal values based on several scenarios given by the software.

3.4.4. Kinetics, ısotherms and thermodynamic study for MB adsorption

Kinetics: The linear plots depicting the three kinetic models for MB adsorption, namely pseudo-first-order, pseudo-second-order, and intraparticle diffusion, can be observed in Figs. 8(a-c). The corresponding calculated parameters are detailed in Table 2. Notably, the R^2 values associated with the pseudo-second-order model approached unity, surpassing the regression coefficients of the other models. This suggests that the pseudo-second-order model provides a superior description of the adsorption kinetics, as evidenced by the close match between the experimental (q_{exp}=53.02) and calculated (q_{cal}=55.55) values derived from this model. The pseudo-

[1] Analysis of Variance (ANOVA)

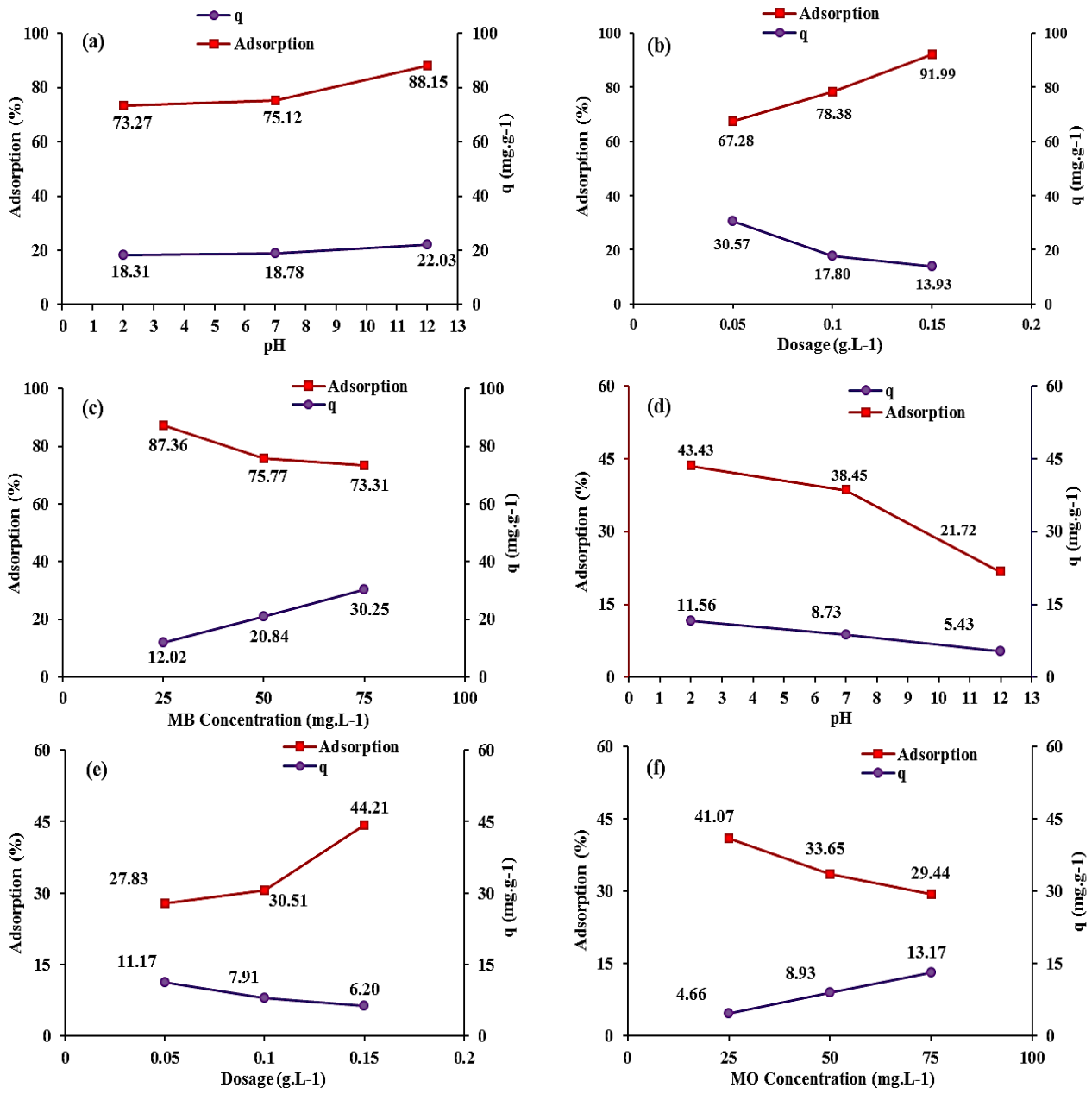

Fig. 7. Effect of pH, adsorbent dosage and dye concentration on adsorption of MB (a-c) and MO (d-f)

second-order model implies a dual-reaction mechanism, with the initial reaction achieving equilibrium rapidly, followed by a slower, prolonged secondary reaction. This model indicates that the adsorption process is contingent upon the availability of surface sites on the adsorbent and that the rate-limiting step involves surface adsorption, specifically chemisorption.

Isotherms: The adsorption isotherms for MB are depicted in Figs. 8(d-f), using the optimal conditions derived from the Taguchi experimental design at concentrations of 20, 40, 60, and 80 mg/L, an adsorbent dosage of 0.05 g, pH of 12, and an equilibrium contact time of 45 minutes. Analysis of the coefficients in Table 3 revealed that the Freundlich model, with a regression coefficient of R^2=0.9915, exhibited a superior fit to the experimental data compared to the Langmuir and Temkin isotherms. The Freundlich equation is applicable to both homogeneous and heterogeneous surfaces, suggesting multilayer adsorption. According to this model, surface concentration never reaches saturation with increasing solute concentration due to the presence of surface sites with high free energy for adsorption. The parameter 'n' in this equation signifies the desirability of adsorption, with values of 'n'>1 indicating a favorable adsorption process and 'n'<1 indicating a weak adsorption potential (Sheikhmali et al., 2024). The value

Table 5. ANOVA table for Taguchi regression model: a) R(%), b) q_t

a) Removal percent as response										
Source	**DF**		**Seq. SS**		**Variance**		**PS**		**Contribution (%)**	
	MB	**MO**	**MB**	**MO**	**MB**	**MO**	**MB**	**MO**	**MB**	**MO**
A	2	2	4.553	61.932	2.276	30.966	4.515	61.554	23.05	57.55
B	2	2	11.072	28.813	5.536	14.406	11.034	28.435	56.32	26.59
C	2	2	3.929	15.829	1.964	7.914	3.891	15.451	19.86	14.45
Error	2	2	0.037	0.377	0.018	0.188				
Total	8	8	19.594	106.954						
b) Adsorption capacity as response										
Source	**DF**		**Seq. SS**		**Variance**		**PS**		**Contribution (%)**	
	MB	**MO**	**MB**	**MO**	**MB**	**MO**	**MB**	**MO**	**MB**	**MO**
A	2	2	4.555	66.204	2.277	33.102	4.518	57.814	2.574	24.19
B	2	2	73.239	39.604	36.619	19.802	73.201	31.215	41.720	13.06
C	2	2	97.637	124.829	48.818	62.414	97.599	116.439	55.620	48.71
Error	2	2	0.036	8.388	0.018	4.194				
Total	8	8	175.469	239.027						

DF: Degree of Freedom, Seq. SS: Sequential Sum of Squares, PS: Pure Sum

Table 6. Optimal conditions for MB and MO adsorption based on R% and q_e

	MB		**MO**	
	(R%)	**q_e (mg/g)**	**(R%)**	**q_e (mg/g)**
pH	12	12	2	2
Adsorbent dosage (g)	0.15	0.05	0.15	0.05
Dye initial Conc. (mg/L)	25	75	25	75
Expected value	114.70	52.80	71.94	25.40
Actual value	98.85	53.29	67.92	22.36

of 'KF' denotes the adsorption capacity, and for this study, a value of 'n'=2.151 indicates the favorable nature of MB adsorption by the adsorbent.

Thermodynamics: The ln K_d versus 1/T plots are shown in Fig. 9 and the thermodynamic parameters computed from these plots are given in Table 7. These parameters provide insights into the spontaneity, feasibility, and nature of the adsorption process The results indicate that the negative Gibbs free energy values across all tested temperatures signify the spontaneous nature of the MB adsorption process on the adsorbent surface. In addition, the values of ΔG° in the range of −20 to 0 kJ/mol indicating that the physisorption is the dominating mechanism in this process. Additionally, the positive enthalpy value suggests that the adsorption process is endothermic, aligning with the observed increase in adsorption with rising temperature. The positive entropy value implies an enhanced likelihood of collision between dye molecules and the adsorbent surface, indicating an increased tendency for the adsorbent to adsorb MB dye molecules through diffusion (Sheikhmali et al., 2024).

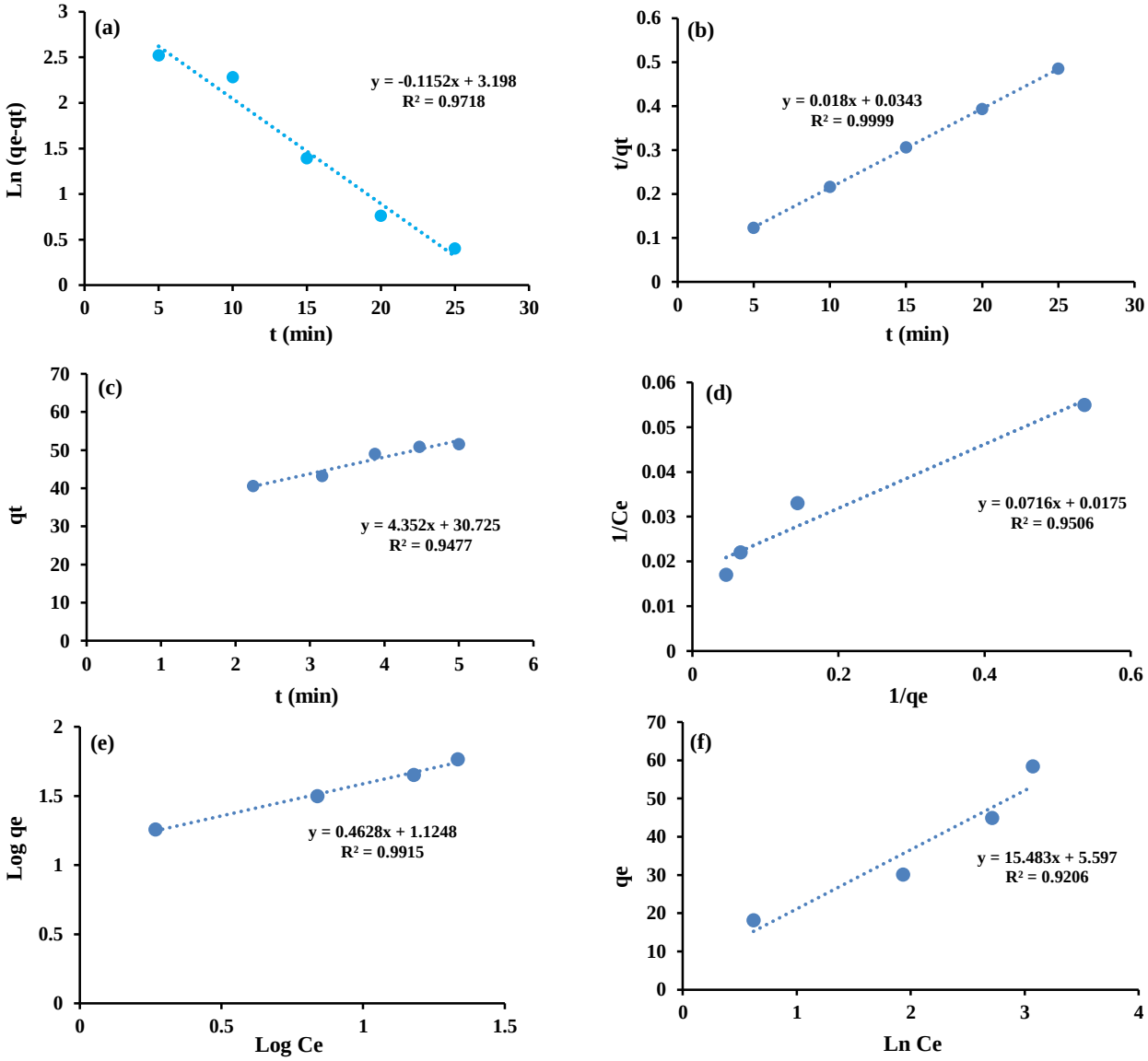

Fig. 8. Linear regression of kinetic models for the MB adsorption process using (a) pseudo-first-order model, (b) pseudo-second-order model, (c) intraparticle diffusion model; and linear regression of isotherm models for the MB adsorption process using (d) Langmuir, (e) Freundlich, and (f) Temkin models

Table 7. Thermodynamic parameters for MB adsorption

T (K)	K_d		ΔG° (KJ/mol)		ΔH° (KJ/mol)		ΔS° (J/mol.K)	
	MB	MO	MB	MO	MB	MO	MB	MO
298	3.799	1.325	-3.307	-2.132	42.169	20.94	152.45	72.483
308	5.408	1.542	-4.322	-1.099				
318	11.012	2.240	-6.342	-0.697				

3.4.5. Kinetics, isotherms and thermodynamics study for MO adsorption

Kinetics: Drawing upon the results outlined in Table 2, it was determined that the R^2 values associated with the pseudo-second-order model surpassed those of other models. Consequently, the adsorption kinetics are more accurately depicted by the pseudo-second-order model.

The coefficients derived from this model indicate that the maximum adsorption capacity of MO on the adsorbent is 21.69 mg/g, with adsorption occurring

through two parallel reactions: a rapid initial reaction followed by a slower reaction that necessitates more time. As per this model, it can be inferred that the chemical adsorption mechanism prevails over physical adsorption and is characterized by a single-layer adsorption process.

Isotherms: The adsorption isotherms illustrate the relationship between the amount of adsorption and the quantity of adsorbate present. Analysis of the results in Table 3 reveals that the R^2 value for the Freundlich isotherm surpasses that of the other two models, suggesting a stronger alignment of this model with the experimental data. Based on this model, it can be inferred that the adsorption process of MO involves unlimited surface coverage and multilayer adsorption on the surface. The inhomogeneity factor n, with a value greater than 1, signifies the favorable nature of MO adsorption by the adsorbent. Furthermore, this model

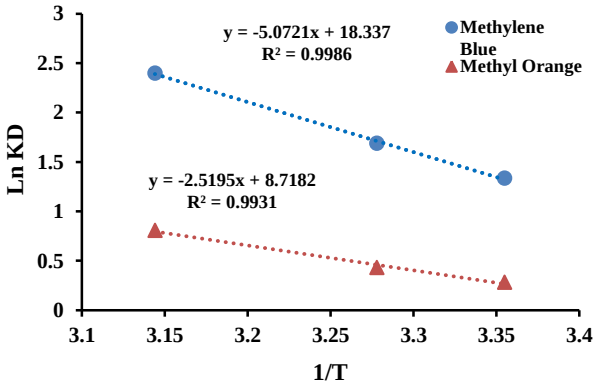

Fig. 9. Linear regression of the Van-Hoff equation to study the thermodynamic behavior of MB and MO adsorption process

does not offer insights into the saturation of the adsorbent surface by the adsorbate.

Thermodynamics: As per the linear diagram depicted in Fig. 9 and the thermodynamic calculations showed in Table 7, the negative Gibbs free energy values observed within the tested temperature range suggest the favorable nature of the adsorption process. Furthermore, the escalation of these values at higher temperatures signifies the heightened affinity of dye molecules and the dehydration reaction with the adsorbent surface, thereby facilitating their interaction and subsequently enhancing adsorption. The positive ΔH° value indicates that the adsorption of MO on the adsorbent is endothermic, implying a robust chemical bond between the dye molecules and the adsorbent surface. Additionally, the positive ΔS° value points towards an increase in disorder and ion exchange, contributing to the stability of the adsorption process and inducing certain structural alterations on the adsorbent surface.

3.5. Mechanistic ınsights and adsorption performance comparison

The superior adsorption performance of the NaOH–ultrasound–modified wheat straw ash arises from combined chemical and physical mechanisms. Alkali treatment removes lignin and hemicellulose, exposes additional –OH and oxygen-containing groups, and increases pore accessibility, as supported by FTIR and BET results. Ultrasound intensifies these effects through acoustic cavitation, where collapsing microbubbles generate microjets and shock waves that fracture cell-wall structures, remove pore-blocking residues, and create new micro-/mesopores, producing a clear synergistic improvement. The higher affinity toward cationic MB is governed by electrostatic attraction between MB^+ and the negatively charged surface (pH_{pzc}=7.5), whereas MO^- experiences partial repulsion. The excellent fit to pseudo-second-order kinetics and the Freundlich isotherm indicates a surface-controlled mechanism involving heterogeneous multilayer adsorption. Thermodynamic parameters (negative ΔG°, positive ΔH° and ΔS°) further confirm that the process is spontaneous, endothermic, and associated with increased interfacial disorder. Together, these mechanisms explain the enhanced adsorption capacity of the modified adsorbent.

The maximum adsorption capacity obtained for MB using the NaOH–ultrasound–modified wheat straw ash (WSA-U-NaOH) in this study (q_{max}=53.29 mg/g) demonstrates a considerable improvement over many low-cost lignocellulosic biosorbents reported in the literature. Untreated or mildly activated agricultural residues such as banana peel, orange peel, and date palm leaves typically exhibit MB adsorption capacities in the range of 20-55 mg/g, placing the performance of WSA-U-NaOH at the upper end of naturally derived adsorbents (Annadurai et al., 2002; Zainol et al., 2022). Even compared with alkali-treated sawdust, sugarcane bagasse, and wheat straw, which generally show q_{max} values between 30–70 mg/g depending on treatment severity, the present adsorbent performs competitively (Hokkanen et al., 2016; Ofomaja, 2008). Although strongly acid-functionalized or highly activated biosorbents such as H_2SO_4-treated coconut shell can reach much higher capacities (up to ~174 mg/g), these materials involve harsher chemicals, higher processing costs, or more complex synthesis routes (Jawad et al., 2020). Thus, the adsorption capacity achieved in this work is notable given the simplicity, low environmental burden, and synergistic effect of combined NaOH and ultrasound modification. These findings highlight that the structural enhancement and increased surface accessibility resulting from alkali–ultrasonic treatment allow WSA-U-NaOH to rival or surpass many conventional low-cost adsorbents reported for MB removal.

Although this study demonstrates the effectiveness of NaOH–ultrasound–modified wheat straw ash for dye removal, further research is needed to evaluate its

regeneration potential, structural stability, and adsorption capacity over multiple reuse cycles. Assessing the adsorbent's performance in real wastewater matrices with competing ions and variable physicochemical conditions would also enhance practical relevance. Future studies may extend the application of this material to additional pollutants such as heavy metals, pharmaceuticals, and emerging contaminants. Moreover, investigations under dynamic conditions (fixed-bed or continuous-flow systems) and preliminary techno-economic assessments of the ultrasonic modification process are recommended to support scale-up and industrial implementation.

4. Conclusion

This study demonstrates that wheat straw and its ash can be effectively transformed into high-performance biosorbents for dye removal through simple and environmentally friendly modification strategies. Among the tested materials, the NaOH–ultrasound–modified wheat straw ash (WSA-U-NaOH) exhibited the highest adsorption performance, achieving maximum capacities of 53.29 mg/g for MB and 22.36 mg/g for MO under optimized conditions determined by the Taguchi design. Kinetic, isotherm, and thermodynamic analyses confirmed that adsorption proceeds through a surface-controlled process with heterogeneous multilayer interactions and occurs spontaneously and endothermically for both dyes. When compared with lignocellulosic biosorbents reported in the literature, WSA-U-NaOH performs competitively and, in many cases, surpasses conventional low-cost agricultural residues, underscoring its potential as an efficient and economically viable adsorbent. The modification approach used in this work offers a practical route for valorizing wheat straw waste while reducing dye pollution in wastewater systems. Future research should focus on exploring regeneration performance, long-term stability, and scale-up potential to broaden the applicability of the developed adsorbent.

References

Abdolkarimi Mahabadi, M. and Bayat, A., 2024. Optimization of the peroxone process for paper industry wastewater treatment using the Box-Behnken design method. *Journal of Water and Wastewater,* 35(1), 40-57. (In Persian). https://dx.doi.org/10.22093/wwj.2023.416748.3371.

Aghaeinejad Meybodi, A., Ebadi, A. and Alamdari, A., 2024. Wastewater treatment of fluoxetine unit of aria pharmaceuticals using catalytic ozonation process: experimental study and optimization. *Journal of Water and Wastewater,* 35(2), 1-21. (In Persian). https://dx.doi.org/10.22093/wwj.2024.444359.3401.

Akar, S. T., Yilmazer, D., Celik, S., Balk, Y. Y. and Akar, T., 2015. Effective biodecolorization potential of surface modified lignocellulosic industrial waste biomass. *Chemical Engineering Journal,* 259, 286-292. https://doi.org/10.1016/j.cej.2014.07.112.

Alizadeh, M., Haghighi, M. and Shabani, M., 2026. Fuel-Driven one-pot microwave-combustion engineering of Z-scheme Cu-Al-CuAl nanophotocatalyst for solar-powered decontamination of textile effluents. *Solar Energy,* 304, 114192. https://doi.org/10.1016/j.solener.2025.114192.

Alizadeh, M., Jalilnejad, E. and Rafiee, R., 2019. Application of hydrogels in adsorptive removal of aqueous pollutants. *Iranian Journal of Polymer Science and Technology,* 31(6), 499-518. (In Persian). https://doi.org/10.22063/jipst.2019.1622.

Alizadeh, M., Peighambardoust, S. J. and Foroutan, R., 2024. Efficacious adsorption of divalent nickel ions over sodium alginate-g-poly(acrylamide)/hydrolyzed Luffa cylindrica-$CoFe_2O_4$ bionanocomposite hydrogel. *International Journal of Biological Macromolecules,* 254, 127750. https://doi.org/10.1016/j.ijbiomac.2023.127750.

Alizadeh, M., Peighambardoust, S. J., Foroutan, R., Azimi, H. and Ramavandi, B., 2022. Surface magnetization of hydrolyzed Luffa Cylindrica biowaste with cobalt ferrite nanoparticles for facile Ni^{2+} removal from wastewater. *Environmental Research,* 212, 113242. https://doi.org/10.1016/j.envres.2022.113242.

Annadurai, G., Juang, R. S. and Lee, D. J., 2002. Use of cellulose-based wastes for adsorption of dyes from aqueous solutions. *Journal of Hazardous Materials,* 92(3), 263-274. https://doi.org/10.1016/S0304-3894(02)00017-1.

Dawi, E. and Padervand, M., 2025. Ag/AgCl-decorated layered lanthanum/niobium oxide microparticles as efficient photocatalysts for Azo Dye remediation and cancer cell inactivation. *Catalysts,* 15(7), 638. https://doi.org/10.3390/catal15070638.

De Quadros Melo, D., De Oliveira Sousa Neto, V., De Freitas Barros, F. C., Raulino, G. S. C., Vidal, C. B. and Do Nascimento, R. F., 2016. Chemical modifications of lignocellulosic materials and their application for removal of cations and anions from aqueous solutions. *Journal of Applied Polymer Science*, 133(15). https://doi.org/10.1002/app.43286.

Deniz, F., 2013. Optimization of methyl orange bioremoval by Prunus amygdalus L. (almond) shell waste: Taguchi methodology approach and biosorption system design. *Desalination and Water Treatment*, 51(37), 7067-7073. https://doi.org/10.1080/19443994.2013.767754.

Forouzandeh-Malati, M., Ganjali, F., Zamiri, E., Zarei-Shokat, S., Jalali, F., Padervand, M. et al., 2022. Efficient photodegradation of eriochrome Black-T by a trimetallic magnetic self-synthesized nanophotocatalyst based on Zn/Au/Fe-embedded poly (Vinyl Alcohol). *Langmuir*, 38(45), 13728-13743. https://doi.org/10.1021/acs.langmuir.2c01822.

Gouamid, M., Ouahrani, M. R. and Bensaci, M. B., 2013. Adsorption equilibrium, kinetics and thermodynamics of methylene blue from aqueous solutions using date palm leaves. *Energy Procedia*, 36, 898-907. https://doi.org/10.1016/j.egypro.2013.07.103.

Guo, Y., Zhu, W., Li, G., Liu, B. and Zhai, D., 2019. Migration of copper with wheat straw in soil under the alternate dry-wet and eluviation conditions. *Communications in Soil Science and Plant Analysis*, 50(12), 1512-1523. https://doi.org/10.1080/00103624.2019.1631330.

Han, G., Deng, J., Zhang, S., Bicho, P. and Wu, Q., 2010. Effect of steam explosion treatment on characteristics of wheat straw. *Industrial Crops and Products*, 31(1), 28-33. https://doi.org/10.1016/j.indcrop.2009.08.003.

Heidarpour, H., Padervand, M., Soltanieh, M. and Vossoughi, M., 2020. Enhanced decolorization of rhodamine B solution through simultaneous photocatalysis and persulfate activation over Fe/C_3N_4 photocatalyst. *Chemical Engineering Research and Design*, 153, 709-720. https://doi.org/10.1016/j.cherd.2019.09.007.

Hemmatzadeh, A. H., Sarrafzadeh, M. H. and Qomi, H. R., 2024. Investigating the performance of cold plasma in removing methylene blue dye from textile wastewater. *Journal of Water and Wastewater*, 35(2), 72-92. (In Persian). https://dx.doi.org/10.22093/wwj.2024.443843.3399.

Hokkanen, S., Bhatnagar, A. and Sillanpää, M., 2016. A review on modification methods to cellulose-based adsorbents to improve adsorption capacity. *Water Research*, 91, 156-173. https://doi.org/10.1016/j.watres.2016.01.008.

Hong, S., Wen, C., He, J., Gan, F. and Ho, Y. S., 2009. Adsorption thermodynamics of methylene blue onto bentonite. *Journal of Hazardous Materials*, 167(1), 630-633. https://doi.org/10.1016/j.jhazmat.2009.01.014.

Hu, D., Liu, S., Qi, L., Liang, J. and Zhang, G., 2024. A critical review on ultrasound-assisted adsorption and desorption technology: mechanisms, influencing factors, applications and prospects. *Journal of Environmental Chemical Engineering*, 12(6), 114307. https://doi.org/10.1016/j.jece.2024.114307.

Idan, I. J., Abdullah, L. C., Choong, T. S. and Jamil, S. N. A. B. M., 2018. Equilibrium, kinetics and thermodynamic adsorption studies of acid dyes on adsorbent developed from kenaf core fiber. *Adsorption Science and Technology*, 36(1-2), 694-712. https://doi.org/10.1177/0263617417715532.

Jain, S. N. and Gogate, P. R., 2017. Adsorptive removal of acid violet 17 dye from wastewater using biosorbent obtained from NaOH and H_2SO_4 activation of fallen leaves of *Ficus racemosa*. *Journal of Molecular Liquids*, 243, 132-143. https://doi.org/10.1016/j.molliq.2017.08.009.

Jalilnejad, E., Alizadeh, M. and Jabbari, B., 2024. Ion-Exchange Membranes in Microbial Fuel Cell Systems. in Basile, A. and Ghasemzadeh, K., eds. *Current Trends and Future Developments on (Bio-) Membranes*: Elsevier. pp. 229-263. https://doi.org/10.1016/B978-0-323-88509-6.00004-6.

Jalilnejad, E., Fakhraddinfakhriazar, S. and Alizadeh, M., 2025. Modeling of Municipal Biological Wastewater Treatment. in Basile, A., Cassano, A. and Ghasemzadeh, K., eds. *Municipal Wastewater Treatment*: Elsevier. pp. 467-510. https://doi.org/10.1016/B978-0-443-24826-9.00014-0.

Jawad, A. H., Abdulhameed, A. S. and Mastuli, M. S., 2020. Acid-factionalized biomass material for methylene blue dye removal: a comprehensive adsorption and mechanism study. *Journal of Taibah University for Science*, 14(1), 305-313. https://doi.org/10.1080/16583655.2020.1736767.

Kecili, R. and Hussain, C. M., 2018. Chapter 4 - Mechanism of Adsorption on Nanomaterials. in Hussain, C. M., ed. *Nanomaterials in Chromatography*: Elsevier. pp. 89-115. https://doi.org/10.1016/B978-0-12-812792-6.00004-2.

Ma, H., Yu, L., Yang, L., Yao, Y., Shen, G., Wang, Y. et al., 2025. Graphene oxide composites for dye removal in textile, printing and dyeing wastewaters: a review. *Environmental Chemistry Letters*, 23(1), 165-193. https://doi.org/10.1007/s10311-024-01794-4.

Ofomaja, A. E., 2008. Kinetic study and sorption mechanism of methylene blue and methyl violet onto mansonia (*Mansonia altissima*) wood sawdust. *Chemical Engineering Journal*, 143(1), 85-95. https://doi.org/10.1016/j.cej.2007.12.019.

Padervand, M., Rhimi, B. and Wang, C., 2021. One-pot synthesis of novel ternary $Fe_3N/Fe_2O_3/C_3N_4$ photocatalyst for efficient removal of rhodamine B and CO_2 reduction. *Journal of Alloys and Compounds*, 852, 156955. https://doi.org/10.1016/j.jallcom.2020.156955.

Ramrakhiani, L., Ghosh, S. and Majumdar, S., 2016. Surface modification of naturally available biomass for enhancement of heavy metal removal efficiency, upscaling prospects, and management aspects of spent biosorbents: a review. *Applied Biochemistry and Biotechnology*, 180(1), 41-78. https://doi.org/10.1007/s12010-016-2083-y.

Salman, M., Athar, M. and Farooq, U., 2015. Biosorption of heavy metals from aqueous solutions using indigenous and modified lignocellulosic materials. *Reviews in Environmental Science and Bio/Technology*, 14(2), 211-228. https://doi.org/10.1007/s11157-015-9362-x.

Sheikhmali, M., Jalilnejad, E. and Rafiee, R., 2024. Synthesis, characterization, experimental design and process analysis of heavy metals adsorption on a wheat straw based amidoximated bioadsorbent. *Scientific Reports*, 14(1), 31083. https://doi.org/10.1038/s41598-024-81982-y.

Silva, L. S., Ferreira, F. J. L., Silva, M. S., Citó, A. M. G. L., Meneguin, A. B., Sábio, R. M. et al., 2018. Potential of amino-functionalized cellulose as an alternative sorbent intended to remove anionic dyes from aqueous solutions. *International Journal of Biological Macromolecules*, 116, 1282-1295. https://doi.org/10.1016/j.ijbiomac.2018.05.034.

Song, W., Yang, Z., Zhang, S., Fei, B. and Zhao, R., 2023. Properties enhancement of poly (β-hydroxybutyrate) biocomposites by incorporating surface-modified wheat straw flour: effect of pretreatment methods. *International Journal of Biological Macromolecules*, 232, 123456. https://doi.org/10.1016/j.ijbiomac.2023.123456.

Tejada-Tovar, C., Villabona-Ortíz, Á. and Gonzalez-Delgado, Á. D., 2021. Adsorption of Azo-anionic dyes in a solution using modified coconut (*Cocos nucifera*) mesocarp: kinetic and equilibrium study. *Water*, 13(10), 1382. https://doi.org/10.3390/w13101382.

Wu, M., Liu, H. and Yang, C., 2019. Effects of pretreatment methods of wheat straw on adsorption of Cd(II) from waterlogged paddy soil. *International Journal of Environmental Research and Public Health*, 16(2), 205. https://doi.org/10.3390/ijerph16020205.

Yaghoobi Rahni, S. and Younesi, H., 2025. One-step synthesis of basic bismuth nitrate and bismuth metal composite (Bi/BBN) to enhance photocatalytic degradation of rhodamine B dye. *Journal of Water and Wastewater*, 36(1), 43-57. (In Persian). https://doi.org/10.22093/wwj.2025.524151.3494.

Yang, Y., Zhu, Q., Peng, X., Sun, J., Li, C., Zhang, X. et al., 2022. Hydrogels for the removal of the methylene blue dye from wastewater: a review. *Environmental Chemistry Letters*, 20(4), 2665-2685. https://doi.org/10.1007/s10311-022-01414-z.

Zainol, N. A., Baharuddin, A., Yusoff, N. A., Sohaimi, K. S. A., Rohaizad, N. M., Ghani, A. A. et al., 2022. Removal of methylene blue dye from aqueous solution by using orange peel treated with acid as an adsorbent. *Desalination and Water Treatment*, 260, 161-168. https://doi.org/10.5004/dwt.2022.28425.

Zhang, Z., Rumi, S. S., Lucia, L. A. and Abidi, N., 2024. Transforming low-quality cotton fibers into dye adsorbents. *Environmental Chemistry Letters*, 22(3), 981-987. https://doi.org/10.1007/s10311-023-01692-1.